Filament-Length-Controlled Elasticity in 3D Fiber Networks

C. P. Broedersz,[1,2,3] M. Sheinman,[1,2] and F. C. MacKintosh[1,2]

[1]*Department of Physics and Astronomy, Vrije Universiteit, Amsterdam, The Netherlands*
[2]*Kavli Institute for Theoretical Physics, University of California, Santa Barbara, California 93106, USA*
[3]*Lewis-Sigler Institute for Integrative Genomics and the Department of Physics, Princeton University, Princeton, New Jersey 08544, USA*

(Received 22 August 2011; published 13 February 2012)

We present a model for disordered 3D fiber networks to study their linear and nonlinear elasticity. In contrast to previous 2D models, these 3D networks with binary crosslinks are underconstrained with respect to fiber stretching elasticity, suggesting that bending may dominate their response. We find that such networks exhibit a bending-dominated elastic regime controlled by fiber length, as well as a crossover to a stretch-dominated regime for long fibers. Finally, by extending the model to the nonlinear regime, we show that these networks become intrinsically nonlinear with a vanishing linear response regime in the limit of flexible or long filaments.

DOI: 10.1103/PhysRevLett.108.078102 PACS numbers: 87.16.Ka, 62.20.de, 83.10.Tv, 83.60.Df

Materials ranging from paper and textiles to the structural components of living cells and tissues [1] consist of networks of fibers or stiff polymers. Such networks have extraordinary mechanical properties [2–4]. Their elasticity depends in part on their connectivity [5,6], in analogy with jammed matter [7,8] and network glasses [9]. The mechanics of the constituent fibers, and specifically their bending rigidity, can also strongly impact network elasticity [10]. However, the relative importance of fiber stretching versus bending is not understood, especially in 3D. Prior work has mostly focused on 2D networks [11–16] since simulations in 3D are challenging and have usually been limited to small system size [17,18]. Significant qualitative differences are expected between 2D and 3D networks: for the typical case of binary fiber interactions, the high molecular weight limit in 2D actually corresponds to the Maxwell central-force (CF) isostatic threshold, where stretching interactions begin to completely constrain network deformations. In contrast, 3D networks with binary interactions remain well below CF isostaticity. Thus, owing to their marginal stability, real 3D fiber networks are expected to be fundamentally more bending dominated and more prone to collective nonaffine deformations [10,18]; even the existence of a simple affine limit dominated by fiber stretching is unknown.

Here we develop a numerical model for the elasticity of random 3D fiber networks with binary crosslinks. This model provides access to network configurations ranging from the rigidity percolation threshold to the previously inaccessible high molecular weight limit. These networks exhibit various qualitatively distinct elastic regimes: a critical regime governed by the rigidity percolation point, a length-controlled bending regime, and an affine stretching regime, as shown in Fig. 1(a). We provide a scaling analysis for insight into the origins of these regimes. Paradoxically, although these networks in 3D can only be rigid with nonzero fiber-bending stiffness, we find that no matter how weak this bending rigidity is, network elasticity approaches an affine limit that is insensitive to fiber bending for high molecular weight. Moreover, in the limit of flexible filaments with weak bending rigidity or high molecular weight, these networks become intrinsically nonlinear with a vanishing linear response regime [Fig. 1(b)].

Much has been learned about stiff polymer gels from minimal models, such as 2D Mikado networks of randomly placed straight filaments with binary crosslinks [11,12]. The elasticity of such Mikado networks is governed by *nonaffine* fiber bending (NAB) deformations at low densities, while higher density networks exhibit predominantly *affine* stretching (AS) elasticity of single fiber segments [11,12]. The crossover from NAB to AS regimes can be understood as being the result of increasing

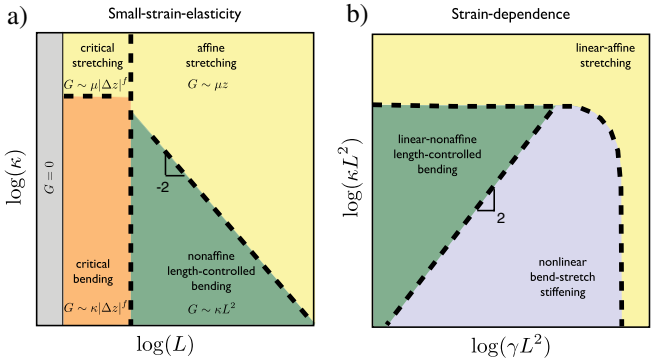

FIG. 1 (color online). Schematic phase diagrams for the linear (a) and nonlinear elasticity (b) of 3D fiber networks on the Ph fcc lattice, where L is the average filament length, z is network connectivity, γ is strain, and κ is the fiber bending rigidity. All lengths are measured in units of the lattice spacing ℓ_0 and κ in units of $\mu\ell_0^2$. The solid boundary line indicates a sharp phase transition and dashed lines indicate a crossover.

fiber length, measured in units of the distance between crosslinks. However, for such 2D networks, this high molecular weight limit actually coincides with Maxwell's CF isostatic connectivity, $z_{CF} = 2d$ in d dimensions [5], which can also give rise to a bend-stretch transition [6,13]; it is thus unclear whether the observed transition in 2D is controlled by CF stretching constraints or by filament length. However, 3D networks with binary crosslinks—characteristic of most biopolymer systems—are qualitatively different; in this case the high molecular weight limit corresponds to network connectivities well below z_{CF}. In the absence of fiber-bending resistance, such networks do not resist shear stresses. Thus, there are reasons to question the existence of an affine, stretching-dominated regime in realistic 3D networks with fibers that are more compliant to bending than to stretching [13,18,19]. This is still the subject of debate since studies in 3D have so far been limited to small systems [18] or to networks with high connectivities [6,19].

To provide insight into the macroscopic mechanics for network configurations ranging from the rigidity percolation point to the high molecular weight limit, we develop a 3D lattice-based fiber network model with binary crosslinks. Our networks consist of straight fibers organized geometrically on a face-centered-cubic (fcc) lattice. However, we limit the maximum coordination number to four by randomly assigning three *independent* pairs of crosslinked fibers out of the six fibers crossing at a vertex. Although the different binary crosslinks may overlap geometrically, they do not constrain each other [20] [inset Fig. 2(a)]. Therefore, we term this the phantom (Ph) fcc lattice. This model is similar to a generalized kagome lattice in 3D [21], although the Ph fcc has a higher symmetry. By cutting bonds with a probability $1 - p$, we tune the average molecular weight, $L = \ell_0/(1 - p)$, where ℓ_0 is the distance between vertices [6,20].

The elastic energy of the 3D Ph fcc network involves stretching and bending contributions of the constituent fibers, characterized by their stretching modulus μ and bending rigidity κ. Each lattice vertex consists of three independent freely hinging binary crosslinks ranked by h. For small displacements, denoted by $\mathbf{u}_i^h$, the stretching energy of the network is expressed as

$$E_S = \frac{1}{2}\frac{\mu}{\ell_0}\sum_{h=1}^{3}\sum_{\langle ij\rangle} g_{ij}^h(\mathbf{u}_{ij}^h \cdot \hat{\mathbf{r}}_{ij})^2, \qquad (1)$$

where the second sum extends over neighboring pairs of vertices, $\mathbf{u}_{ij}^h = \mathbf{u}_j^h - \mathbf{u}_i^h$ and $\hat{\mathbf{r}}_{ij}$ is the bond direction in the undeformed lattice. Bond dilution is implemented by setting $g_{ij}^h = 1$ for present bonds and $g_{ij}^h = 0$ for removed bonds. Fibers form straight chains that resist angular deflections, leading to a total bending energy [6,15],

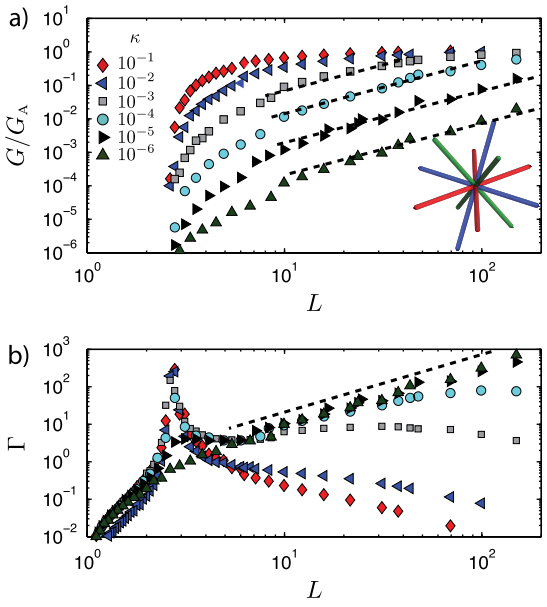

FIG. 2 (color online). (a) The shear modulus as a function of L in units of ℓ_0 for various κ in units of $\mu\ell_0^2$. Here, G_A represents the affine shear modulus of the undiluted Ph fcc lattice. The inset illustrates the phantom principle: at each lattice vertex three independent binary crosslinks are formed between randomly chosen fiber pairs labeled by color. (b) Nonaffinity parameter Γ as a function of L. Dashed black lines indicate a slope of 2.

$$E_B = \frac{1}{2}\frac{\kappa}{\ell_0^3}\sum_{h=1}^{3}\sum_{\langle ijk\rangle} g_{ij}^h g_{jk}^h[(\mathbf{u}_{ij}^h - \mathbf{u}_{jk}^h) \times \hat{\mathbf{r}}_{ij}]^2. \qquad (2)$$

Since the crosslinks themselves do not contribute a torsional stiffness, the second sum only extends over *coaxial* nearest neighbor triplets along the same fiber.

The shear modulus G is determined numerically by applying a shear strain along the 111 plane with Lees-Edwards periodic boundary conditions and energy minimizations are performed by a conjugate gradient algorithm. Our network sizes range from $W^3 = 20^3$ to 150^3 unit cells, with up to 3 times that many crosslinks. Filaments that span the network make unphysical stretch contributions to the elasticity of the sample and may render the deformation field of the network more affine. To avoid such trivial finite size effects, at least one bond is removed along every fiber. Consequently, this model can only approach $z = 4$ asymptotically from below.

Linear regime.—We find numerically that these networks have a finite shear rigidity only if $\kappa > 0$, even though the perfect, undiluted Ph fcc lattice ($z = 4$) deforms affinely and has a finite shear modulus for $\kappa = 0$, similar to the model in Ref. [21].

For finite κ, the Ph fcc networks can be either bending dominated ($G \sim \kappa$ at low κ), or stretching dominated ($G \sim \mu$ at high κ or large L), as shown in Fig. 2(a). Interestingly, there appear to be two distinct regimes well above the rigidity percolation point: a bending-dominated

regime where G depends on L and κ (low κ and L) and an L- and κ-independent stretching-dominated regime (high κ and L). These observations are consistent with those obtained in Ref. [21].

These results can be understood as follows. In the high-κ limit, the network deforms increasingly affinely, with a shear modulus $G \simeq G_A$. Here, $G_A \sim \frac{\mu}{\ell_0^2} z$ is the affine shear modulus, which is completely determined by fiber stretching. However, in the critical regime—controlled by the bending rigidity percolation point z_b—G vanishes continuously with $\Delta z = z - z_b$ [6,9,12,21] as

$$G_{\rm cs} \sim \frac{\mu}{\ell_0^2} |\Delta z|^f, \qquad G_{\rm cb} \sim \frac{\kappa}{\ell_0^4} |\Delta z|^f, \tag{3}$$

for high and low κ, respectively. We find $z_b \approx 2.4$ and $f \approx 0.65$ for a system size $W^3 = 30^3$, as demonstrated in the lower inset in Fig. 3 by showing that $G|\Delta z|^{-f}/\kappa$ reaches a plateau for low values of Δz. The rigidity threshold is similar to observations in prior 3D models [18], although f is considerably lower here, which is more consistent with findings on the generalized 3D kagome lattice [21]. The rigidity threshold can be estimated by a counting argument [5,6,18]; this connectivity threshold occurs when per crosslink the number of stretching constraints, $n_b z/4$, and bending constraints, $n_b(d-1)z^2/16$, equal the number of internal degrees of freedom d. Here, the number of bonds per crosslink $n_b = 2$ in the undiluted network ($z = 4$). This yields $z_b \approx 2.6$, in reasonable agreement with the numerical results.

Since the CF isostatic point lies beyond the physical connectivity range of this model, a naive expectation may be that a nonaffine bending regime extends over the whole range $z < 4$ for low κ, such that $G \ll G_A$ as $z \to 4$ from below. However, this argument ignores possible effects due to filament length. In networks of straight fibers with binary interactions, the average fiber length diverges as $z \to 4$ and large L may lead to nonaffine displacements over greater length scales [13]. The effects of high L on the deformation field have been discussed in the context of 2D Mikado networks using both scaling arguments [11,12] and floppy mode theory [13], although the corresponding effects in 3D are unknown.

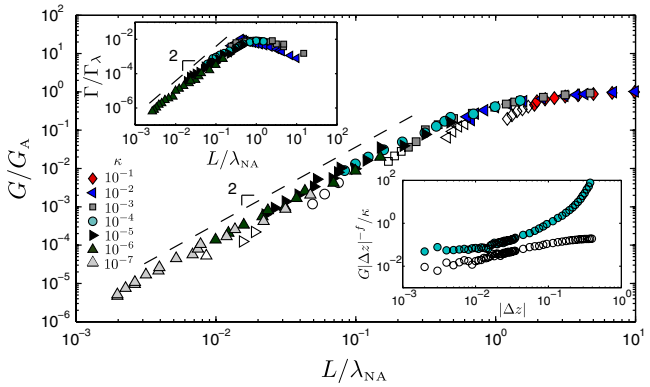

FIG. 3 (color online). The shear modulus scaled with the affine modulus G_A versus L scaled with $\lambda_{\rm NA} = \ell_0^2/\ell_b$ for various values of κ in units of $\mu\ell_0^2$. The open symbols indicate data ranges in the rigidity percolation regime where we observe different scaling. The lower inset shows G scaled with $|\Delta z|^f$ as a function of $|\Delta z|$ and here the open circles correspond to $\kappa = 1$. The upper inset shows the nonaffine fluctuations Γ scaled with $\Gamma_\lambda = \lambda_{\rm NA}/\ell_0^2$ versus $L/\lambda_{\rm NA}$.

Here, we investigate the effects of molecular weight on the deformation field and their implications for the mechanics of 3D fiber networks. Network nodes along a fiber can undergo independent nonaffine deformations scaling as γL to avoid stretching of the other fibers to which they are connected. This direct scaling of nonaffine displacements with L was proposed in Ref. [13] and constitutes one of the central assumptions of the floppy mode model that was applied to Mikado networks. To test this assumption, we investigate the strain fluctuations using the nonaffinity measure [6,11,22], $\Gamma = \frac{1}{\ell_0^2 \gamma^2} \langle (\delta \mathbf{u}^{\rm NA})^2 \rangle$, where $\delta \mathbf{u}^{\rm NA} = \mathbf{u} - \mathbf{u}^{\rm A}$ denotes the nonaffine displacement of a crosslink and the brackets represent a network average. This nonaffinity measure exhibits a cusp at the bending rigidity percolation point, reflecting the criticality of the network's mechanics in this regime [6,7], as shown in Fig. 2(b). Furthermore, there appears to be a regime for sufficiently low κ where $\Gamma \sim L^2$ independent of κ, lending credence to the basic assumption that $\delta u^{\rm NA} \sim L\gamma$ [13].

Such length-controlled nonaffine deformations store an amount of elastic energy scaling as $\kappa(\delta u^{\rm NA}/\ell_0^2)^2 \ell_0$ per segment, which on the macroscopic level results in a shear modulus for this bending regime,

$$G_{\rm LC} \sim \frac{\kappa}{\ell_0^2} \left(\frac{\delta u^{\rm NA}}{\ell_0^2} \right)^2 \frac{1}{\gamma^2} \sim \frac{\kappa}{\ell_0^6} L^2. \tag{4}$$

This prediction for the L dependence of G is born out by the numerical data, as shown in Fig. 2(a). This analysis further implies that the energetic cost of nonaffine bending deformations grows with increasing L. As a result, such nonaffine bending deformations become less favorable than the L-independent affine stretching deformations when the average molecular weight exceeds a nonaffinity length scale, $\lambda_{\rm NA}$. This crossover length scale can be estimated by comparing $G_{\rm LC}$ with the affine stretching shear modulus G_A, which forms an upper bound to the shear modulus; this gives

$$\lambda_{\rm NA} = \ell_0^2/\ell_b, \tag{5}$$

where $\ell_b = \sqrt{\kappa/\mu}$. Indeed, by plotting G/G_A as a function of $L/\lambda_{\rm NA}$ we find a collapse of the data to a universal curve, for which $G/G_A \simeq$ when $L/\lambda_{\rm NA} \gtrsim 1$, as shown in Fig. 3. This supports the existence of a NAB-AS transition driven by molecular weight in 3D fiber networks with connectivities well below Maxwell's CF isostatic point. In contrast, prior results for 2D networks suggested $\lambda_{\rm NA} \sim \ell_b^{-\alpha}$, with $\alpha \approx 0.3$–0.4 [11,12]. However, for such

networks it is unclear whether the NAB-AS transition is actually driven by fiber length, as for the 3D case presented here, or by the CF isostatic point [6,13] that coincides with the high-L limit for the Mikado model. A similar scaling analysis can be performed for the nonaffine fluctuations [Fig. 2(b)]. At the crossover $\Gamma = \Gamma_\lambda = \lambda_{\rm NA}^2/\ell_0^2 = \ell_0^2/\ell_b^2$ and thus, we can collapse the nonaffinity data above the critical regime by plotting Γ/Γ_λ as a function of $L/\lambda_{\rm NA}$, as shown in the upper inset of Fig. 3. This shows that Γ/Γ_λ reaches a maximum at the NAB-AS crossover followed by a gradual decrease with $L/\lambda_{\rm NA}$. We summarize the conclusions for the various elastic regimes based on this scaling analysis and the raw data (Fig. 2) in Fig. 1(a), in which the crossovers are indicated by dashed lines.

Nonlinear regime.—The length-controlled bending mechanics also has important implications for the nonlinear elasticity of 3D fiber networks. Even in a bending-dominated regime, stretching modes are excited at finite network deformations [14], but to a higher order in the applied strain [7,10,13]. Specifically, assuming length-controlled nonaffine deformations, a transverse bend with an amplitude $\sim\gamma L$ results in a stretch energy in the associated bond, $\delta E_S \sim \mu\epsilon^2\ell_0$, where $\epsilon \sim (\gamma L/\ell_0)^2 + O(\gamma^4)$. The onset of nonlinear network elasticity occurs at a strain γ_0, at which δE_S becomes comparable to the bending contribution, $\delta E_B \sim \kappa L^2\gamma^2/\ell_c^3$. This stiffening saturates at a strain γ_A, set by the condition $\delta E_B + \delta E_S \sim \frac{\mu}{\ell_0^2}\gamma^2$, at which the network's response becomes dominated by affine stretching modes. Thus, the onset and completion of the stiffening regime are expected to scale as

$$\gamma_0 \sim \frac{\ell_b}{L}, \qquad \text{and} \qquad \gamma_A \sim \frac{\ell_0^2}{L^2}\sqrt{1 - L^2\ell_b^2/\ell_0^4}. \qquad (6)$$

Here we focus on the characteristic strain for the onset of nonlinear behavior, γ_0, which is shown in Fig. 4(b). To further test the scaling prediction, we collapse the data by plotting $(\ell_b L)^2$ as a function of the scaled characteristic strain $\gamma_0 L^2$ (inset Fig. 4). Importantly, these results provide evidence for a vanishing linear response regime in the limits $\kappa \to 0$ and $L \to \infty$. The scaling of the nonlinear behavior of the network is illustrated in the schematic phase diagram in Fig. 1(b).

Using the phantom model together with a scaling analysis, we have shown that even though the mechanical stability of 3D networks relies on the bending resistance of the constituent fibers, surprisingly for any $\kappa > 0$, network mechanics becomes affine and independent of κ when $L > \lambda_{\rm NA}$. We conjecture that main results of this Letter also apply to models with additional interactions other than fiber bending, which stabilize the network below the CF threshold, including next-nearest-neighbor interactions or bond-bending interactions for crosslinks that fix a preferred bond angle. Specifically, such networks should exhibit an affine high molecular weight limit and a vanishing linear elastic regime in the limit of long filaments or weak interactions [7].

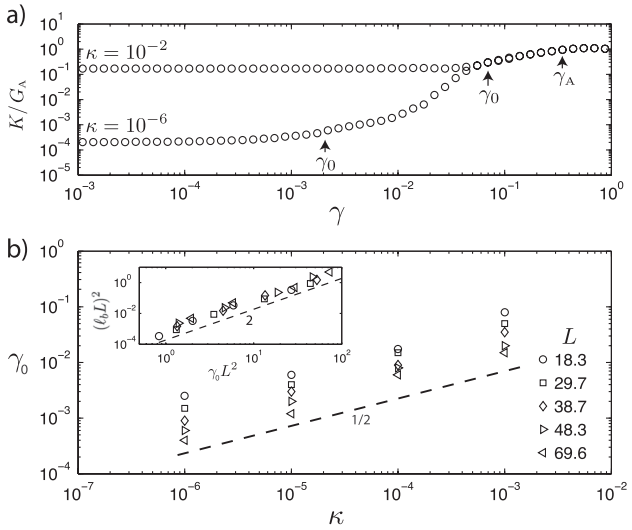

FIG. 4. (a) The differential modulus $K = d\sigma/d\gamma$ scaled by the affine modulus G_A, together with γ_0 and γ_A for networks with $L = 18.3$. (b) Characteristic strain for the onset of nonlinear behavior. The inset shows the collapse according to the scaling prediction in Eq. (6). L is measured in units of ℓ_0 and κ in units of $\mu\ell_0^2$.

The scaling analysis presented here for athermal fiber networks may also be used to develop predictions for thermal systems for which the crosslinking length scale is expected to scale with $\rho^{-2/5}$ [23], where ρ is the polymer length density. In the bending regime, we expect $G \sim \kappa\rho^{13/5}$ for thermal semiflexible polymers and $G \sim \kappa\rho^3$ for stiff fibers. These predictions may account for a recent report of $G \sim \rho^{2.68}$ in collagen networks [17].

The Ph fcc model developed here provides a powerful numerical model to probe the mechanics of 3D fiber networks with large system sizes. This model can also be extended to study the dynamic network rheology and the effects of force generating molecular motors.

This research was supported by the National Science Foundation under Grant No. NSF PHY05-51164 and by FOM/NWO. It is a pleasure to acknowledge discussions with E. Frey, M. Das, C. Heussinger, O. Stenull, and T. C. Lubensky. We also thank O. S. and T. C. L. for sharing their manuscript (Ref. [21]) prior to publication.

[1] D. A. Fletcher and R. D. Mullins, Nature (London) **463**, 485 (2010).
[2] P. A. Janmey, S. Hvidt, J. Lamb, and T. P. Stossel, Nature (London) **345**, 89 (1990).
[3] A. R. Bausch and K. Kroy, Nature Phys. **2**, 231 (2006).
[4] P. A. Janmey *et al.*, Nature Mater. **6**, 48 (2007).
[5] J. C. Maxwell, Philos. Mag. **27**, 294 (1864).
[6] C. P. Broedersz, X. Mao, T. C. Lubensky, and F. C. MacKintosh, Nature Phys. **7**, 983 (2011).

[7] M. Wyart, H. Liang, A. Kabla, and L. Mahadevan, Phys. Rev. Lett. **101**, 215501 (2008).
[8] A. J. Liu and S. R. Nagel, Nature (London) **396**, 21 (1998).
[9] M. F. Thorpe, J. Non-Cryst. Solids **57**, 355 (1983).
[10] O. Lieleg, M. M. A. E. Claessens, C. Heussinger, E. Frey, and A. R. Bausch, Phys. Rev. Lett. **99**, 088102 (2007).
[11] D. A. Head, A. J. Levine, and F. C. MacKintosh, Phys. Rev. Lett. **91**, 108102 (2003); Phys. Rev. E **68**, 061907 (2003).
[12] J. Wilhelm and E. Frey, Phys. Rev. Lett. **91**, 108103 (2003).
[13] C. Heussinger and E. Frey, Phys. Rev. Lett. **97**, 105501 (2006); C. Heussinger, B. Schaefer, and E. Frey, Phys. Rev. E **76**, 031906 (2007).
[14] P. R. Onck, T. Koeman, T. van Dillen, and E. van der Giessen, Phys. Rev. Lett. **95**, 178102 (2005).
[15] M. Das, F. C. MacKintosh, and A. J. Levine, Phys. Rev. Lett. **99**, 038101 (2007).
[16] A. R. Missel, M. Bai, W. S. Klug, and A. J. Levine, Phys. Rev. E **82**, 041907 (2010).
[17] S. B. Lindström, D. A. Vader, A. Kulachenko, and D. A. Weitz. Phys. Rev. E **82**, 051905 (2010); A. M. Stein, D. A. Vader, D. A. Weitz, and L. Sander, Complexity **16**, 22 (2011).
[18] E. M. Huisman, T. van Dillen, P. R. Onck, and E. Van der Giessen, Phys. Rev. Lett. **99**, 208103 (2007); E. M. Huisman and T. C. Lubensky, Phys. Rev. Lett. **106**, 088301 (2011).
[19] G. A. Buxton and N. Clarke, Phys. Rev. Lett. **98**, 238103 (2007).
[20] C. P. Broedersz and F. C. MacKintosh, Soft Matter **7**, 3186 (2011).
[21] O. Stenull and T. C. Lubensky, arXiv:1108.4328.
[22] B. A. DiDonna and T. C. Lubensky, Phys. Rev. E **72**, 066619 (2005).
[23] F. C. MacKintosh, J. Käs, and P. A. Janmey, Phys. Rev. Lett. **75**, 4425 (1995).